Simple and mild biomolecule-assisted green route to nanosheet-built zinc indium sulphide microspheres

Wen Cai[1,2], Aiwu Wang[2], Tingke Rao[2], Jie Hu[3], Li Fu[4], Jiasong Zhong[1], Weidong Xiang[1]

[1]*School of Materials Science and Engineering, Tongji University, Shanghai 201804, People's Republic of China*
[2]*Department of Physics and Materials Science, City University of Hong Kong, Hong Kong SAR, People's Republic of China*
[3]*Department of Electrical Engineering, KU Leuven, 3001 Leuven, Belgium*
[4]*Department of Chemistry and Biotechnology, Faculty of Science, Engineering and Technology, Swinburne University of Technology, Hawthorn, VIC, Australia*
E-mail: weidongxiang01@163.com

Published in Micro & Nano Letters; Received on 24th August 2014; Revised on 26th November 2014; Accepted on 3rd December 2014

A simple and mild green route has been developed to synthesise zinc indium sulphide nanopowders with L-cysteine as the sulphur source and complexing agent under hydrothermal conditions at 160 °C for 12 h. The crystal structure, morphologies and chemical composition of the obtained nanopowders are confirmed by X-ray powder diffraction, field-emission scanning electron microscopy, energy dispersive spectrometry, transmission electron microscopy and selected area electron diffraction. Results reveal that the synthesised nanopowder is comprised of microspheres with nanosheets and the diameter of the microspheres and the thickness of the nanosheets are 100 nm–2 μm and 10–50 nm, respectively. Moreover, a possible formation mechanism for the zinc indium sulphide product is briefly discussed. The present route would provide an alternative strategy to prepare other II–III–VI ternary metal sulphide nanocrystals.

1. Introduction: II–III–VI ternary semiconductors are good photo-absorbers for solar cell or photoelectrochemical devices because of the fact that their energy band gaps are in the range of 1.4–2.8 eV [1]. $ZnIn_2S_4$ is one kind of visible light active II–III–VI photo-absorber material, and mostly used as a photocatalyst [2]. The indirect band gap of $ZnIn_2S_4$ lies between 1.8 and 2.1 eV, which matches reasonably well with the solar spectrum for energy conversion. The nano or micrometre $ZnIn_2S_4$ with various morphologies, including nanoparticles [2], tubes, ribbons and wires [3], porous sub-microspheres [4] and flowering-cherry-like microspheres [5], have been reported. Most of the researchers, for instance Gou [3], Shen [6–8], Li [9], Shi [10] and Chai [11] synthesised the $ZnIn_2S_4$ nanopowder by using the simple and mild hydro/solvothermal route. Although great efforts have been made for the synthesis route, the development of a simple, inexpensive, efficient, green and reliable method for the large-scale fabrication of $ZnIn_2S_4$ nanostructures has met with little success. Recently, much attention has been paid to preparing various inorganic nanostructures with the assistance of biomolecules, for example D-penicillamine [12], glutathione [13, 14], glycine [15], L-arginine [16] and protein [17]. Among the numerous biomolecules, L-cysteine has attracted considerable attention and has been used not only as a sulphur source but also as a complexing agent and as a structure directing molecule to control the size and shape of metal sulphide nanostructures because of its multifunctional groups (−SH, $-NH_2$ and −COO−), which can be utilised for the conjugation of metallic ions. For instance, CuS [18], PbS [19] and FeS [20] nanostructures, porous 3D flowerlike β-In_2S_3 structures [21], MoS microspheres with nanorods [22], MnS [23] and CoS [24] hollow microspheres, $AgBiS_2$ microcrystals [25] and layered MoS_2/graphene composites [26] have been synthesised via the L-cysteine-assisted hydro/solvothermal routes. Here we report a simple and mild hydrothermal method for the fabrication of nanosheet-built $ZnIn_2S_4$ microspheres with the assistance of L-cysteine. The introduction of L-cysteine as the sulphide source and distilled water as the solvent, instead of other sulphide sources (e.g. sulphide powder, Na_2S, $Na_2S_2O_3$ etc.) and organic solvents (e.g. DMF, methanol etc.), avoids the yield of toxic by-products. It is worth noting that the present synthetic approach is inexpensive and green and can be used to prepare other II–III–VI ternary metal sulphides.

2. Experimental

2.1. Preparation of nanosheet–built $ZnIn_2S_4$ microspheres: In a typical preparation, analytically pure $ZnCl_2{\cdot}2H_2O$ (0.5 mmol), $InCl_3$ (absolute, 1 mmol) and $C_3H_7NO_2S$ (L-cysteine, 2 mmol) were added to 90 mL of distilled water at room temperature under constant magnetic stirring. Then this mixture solution was transferred into a Teflon-lined autoclave with 100 ml capacity and sealed, then kept at 160 °C for 12 h before the autoclave was cooled down naturally to room temperature. The yellowish precipitate was collected, washed several times by absolute ethanol and distilled water in sequence, then it was dried in a vacuum at 60 °C for 5 h and the obtained nanopowders were collected for characterisation. The yield of the product was 85–90%. Fig. 1 shows the schematic flow-chart for the L-cysteine-assisted hydrothermal synthesis of the $ZnIn_2S_4$ sample.

2.2. Characterisations: The as-synthesised nanopowders were analysed by X-ray powder diffraction (XRD) on a Bruker D8 Advance diffractometer (40 kV, 40 mA) using Cu Kα radiation ($\lambda = 0.15406$ nm) at a scanning rate of 0.02°/s. X-ray photoelectron spectra (XPS) analysis was taken on a Kratos AXIS ULTRADLD X-ray photoelectron spectrometer using Monochrome Al Ka as the excitation source. Field-emission scanning electron microscopy (FE-SEM) was performed on a JEOL instrument (JEOL-6700F) at an accelerating voltage of 10 kV. Energy dispersive spectrometry (EDS) analysis of the nanopowders was carried out on an OXFORD INCA instrument attached to the scanning electron microscope at a scanning range of 0–20 kV to find the chemical composition. The transmission electron microscopy (TEM) image and selected area electron diffraction (SAED) pattern were recorded using a G2F20 microscope (Tecnai, 200 kV). All measurements were carried out at room temperature.

3. Results and discussion: The crystal structure and phase composition of the $ZnIn_2S_4$ nanopowders were tested by XRD.

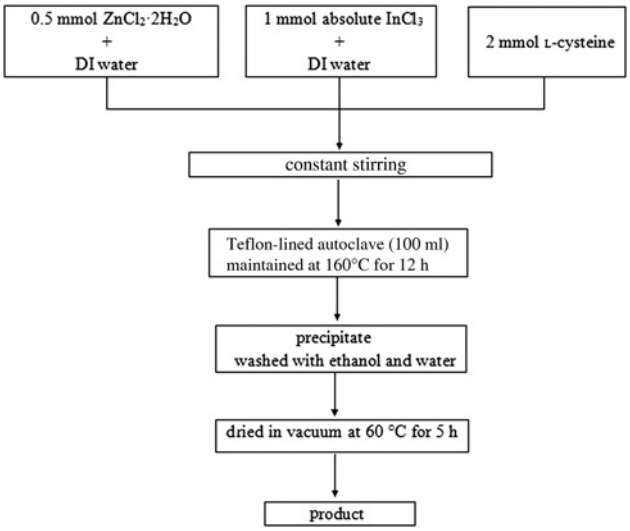

Figure 1 *Flow-chart for L-cysteine-assisted hydrothermal synthesis of $ZnIn_2S_4$ sample*

Fig. 2 displays the XRD pattern of the zinc indium sulphide sample obtained at 160 °C for 12 h. All the diffraction peaks match $ZnIn_2S_4$, which can be indexed with the literature value of the hexagonal phase $ZnIn_2S_4$ (JCPDS Card No. 65-2023, $a = 3.84$ Å, $c = 24.66$ Å). No other diffraction peaks of impurities are observed in the XRD pattern, indicating that pure $ZnIn_2S_4$ has been obtained under the present hydrothermal conditions.

The chemical composition and purity of the obtained $ZnIn_2S_4$ nanopowders were further analysed with XPS. A survey spectrum of the product, shown in Fig. 3*a,* indicates the presence of Zn, In and S as well as C and O impurity. Carbon and oxygen in the product may come from the reference and adsorbed gaseous molecules, respectively. High-resolution spectra were also taken for the Zn 2p region, the In 3d region and the S 2p region so as to determine the valency state and atomic ratio. The Zn 2p core level spectrum shown in Fig. 3*b* indicates that the observed values of the binding energies for Zn $2p_{3/2}$ is 1022 eV, which is almost in accordance with the reported literature values [27]. The peaks around 445.1 and 452.7 eV agree well with the binding energy of In $3d_{5/2}$ and In $3d_{3/2}$ of $ZnIn_2S_4$ (Fig. 3*c*), respectively [27]. The peak at 161.8 eV agrees well with the binding energy of S 2p of $ZnIn_2S_4$ (Fig. 3*d*) [27].

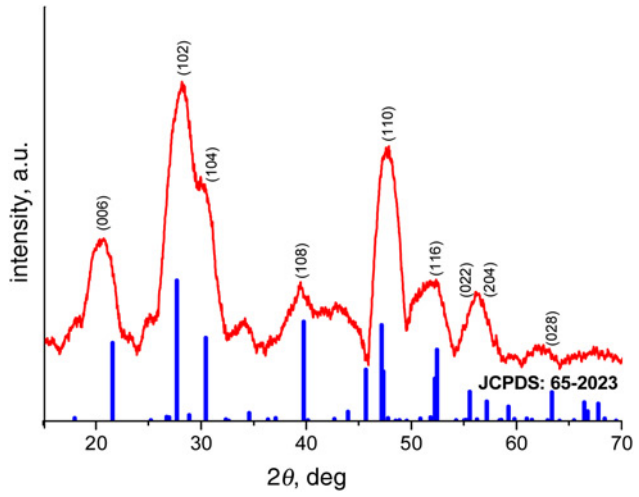

Figure 2 *XRD pattern of the obtained $ZnIn_2S_4$ sample synthesised by a L-cysteine-assisted hydrothermal route*

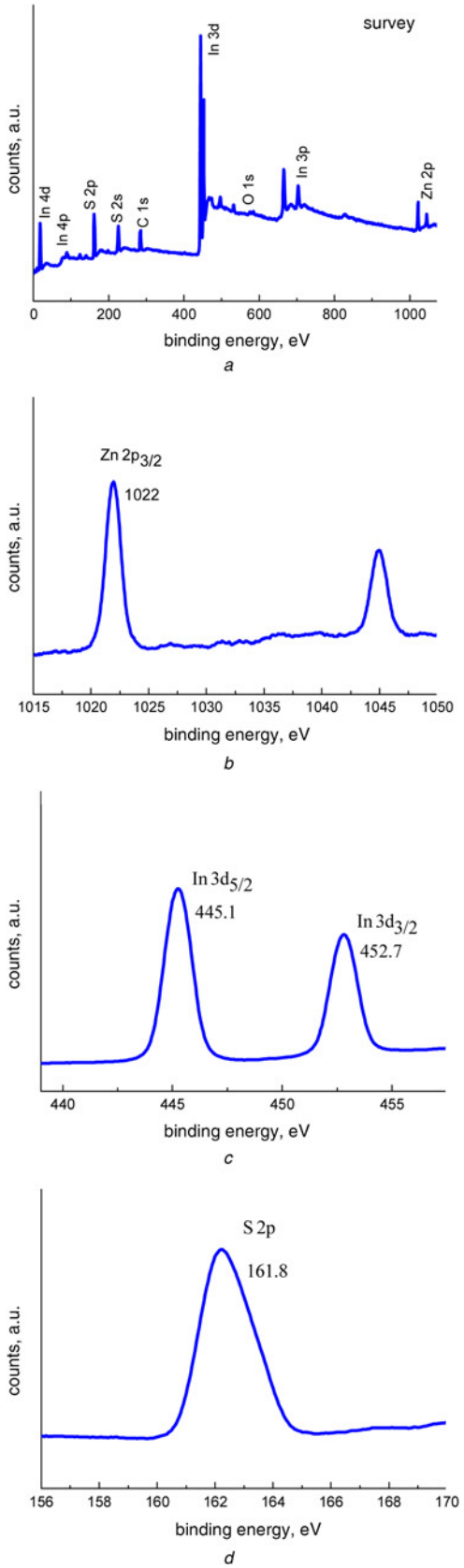

Figure 3 *XPS spectra of $ZnIn_2S_4$ sample*
a Typical XPS survey spectrum of the $ZnIn_2S_4$ sample
b Core level spectrum for Zn 2p
c Core level spectrum for In 3d
d Core level spectrum for S 2p

The morphologies and size of the sample were tested by FE-SEM. Fig. 4 is the typical FE-SEM image of the $ZnIn_2S_4$

doi: 10.1049/mnl.2014.0472

product. The low magnification image (Fig. 4*a*) demonstrates clearly that the sample comprises a large quantity of microspheres with diameters of 100 nm–2 µm. Further observation based on the FE-SEM magnification (Fig. 4*b*) reveals that the microspheres contain large a number of nanosheets with 10–50 nm thickness (inset Fig. 4*b*). The chemical composition of the $ZnIn_2S_4$ microspheres was further confirmed by means of energy dispersive X-ray spectroscopy (EDS), shown in Fig. 4*c*. There are only peaks of Zn, In and S elements in the EDS spectrum, besides the Cu signal arising from the copper TEM grid and the normal C and O peaks. This result is in accordance with the XRD and XPS patterns shown above, which further indicate the high purity of the product.

The morphologies and microstructure of the as-synthesised sample were further characterised by TEM and SAED. Fig. 5*a* illustrates the TEM image of $ZnIn_2S_4$ microspheres, which is well in accordance with the FE-SEM image. Fig. 5*b* is the enlarged TEM image of a single microsphere; a large number of unequal nanosheets that assembled into fringes of the $ZnIn_2S_4$ microspheres can be seen. The SAED pattern (inset Fig. 5*a*) indicates that the $ZnIn_2S_4$ products are polycrystalline in nature. The crystallinity of the $ZnIn_2S_4$ product was further confirmed by the HRTEM. The HRTEM image shown in Fig. 5*c* clearly indicates that the lattice fringes are separated by a spacing of 0.294 nm, which agrees well with the (104) lattice index of hexagonal $ZnIn_2S_4$ (JCPDS Card No. 65-2023, d (104) = 0.29333 nm).

The possible formation mechanism for the nanosheet-built $ZnIn_2S_4$ microspheres is proposed based on the experimental results and [18–25, 28–33]. The growth process for the nanosheet-built $ZnIn_2S_4$ microspheres involves two stages: an initial nucleating step and a following crystal growth step.

For the initial nucleating step, the coordination interaction between Zn^{2+}, In^{3+} ions and L-cysteine undoubtedly play an important role although the exact formation mechanisms for the L-cysteine-assisted hydrothermal preparation of the nanosheet composed of $ZnIn_2S_4$ microspheres are still under investigation. The function groups, for example $–NH_2$, –COOH and –SH, in the L-cysteine molecule have a strong tendency to complex with inorganic metal cations, which has been demonstrated by Burford and co-workers on the basis of the observation from mass spectrometry [28]. First, when mixing L-cysteine with the Zn^{2+} and In^{3+} ions solution, Zn^{2+} and In^{3+} ions coordinate with the L-cysteine molecule to form precursor complexes ($(In(L\text{-cysteine})_n^{3+}$, $Zn(L\text{-cysteine})_n^{2+}$) via the combination of metal cation and the thiol chain. This process prevented the formation of ZnS and In_2S_3 because few free ions (S^{2-}, Zn^{2+} and In^{3+}) were in the solution. Secondly, the L-cysteine molecules were attacked by the strong nucleophilic O atoms in the H_2O molecules at a higher temperature (such as 160 °C) [18], and the precursor complexes were thus broken to release S^{2-}anions, which reacted with the In^{3+} and Zn^{2+} ions to produce $ZnIn_2S_4$ nuclei. At this step, the relative stability of the precursor complexes caused the thermal decomposition to procede more slowly and thus generated a few nuclei in the solution, which is important for the subsequent formation of uniform $ZnIn_2S_4$ microspheres. The reactions involved in the formation step of $ZnIn_2S_4$ nuclei can be written as the following chemical

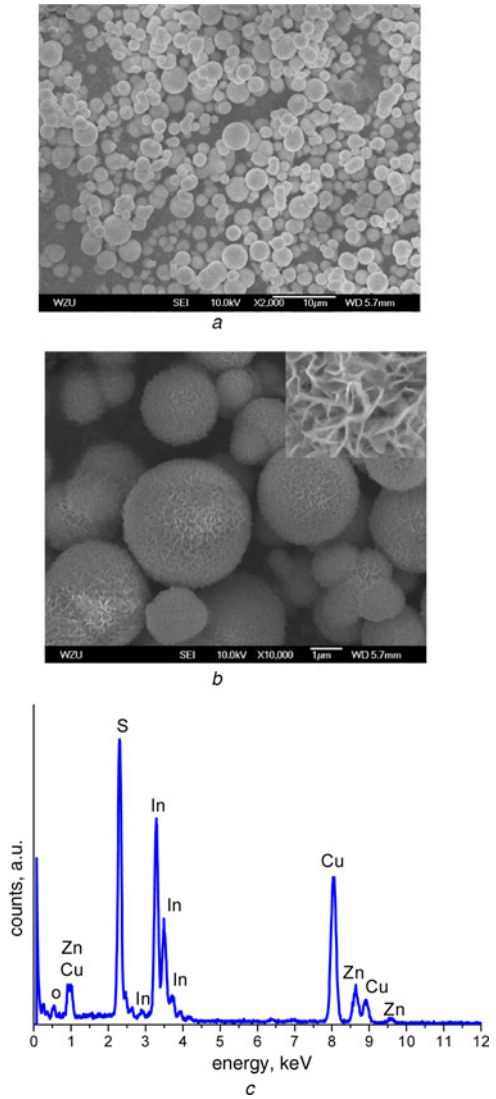

Figure 4 *Representative FESEM images of as-prepared $ZnIn_2S_4$ sample (Figs 4a, b): low magnification (Fig. 4a) and high magnification (Fig. 4b); EDS spectrum (Fig. 4c) (characteristic peaks for Zn, In and S are observed)*

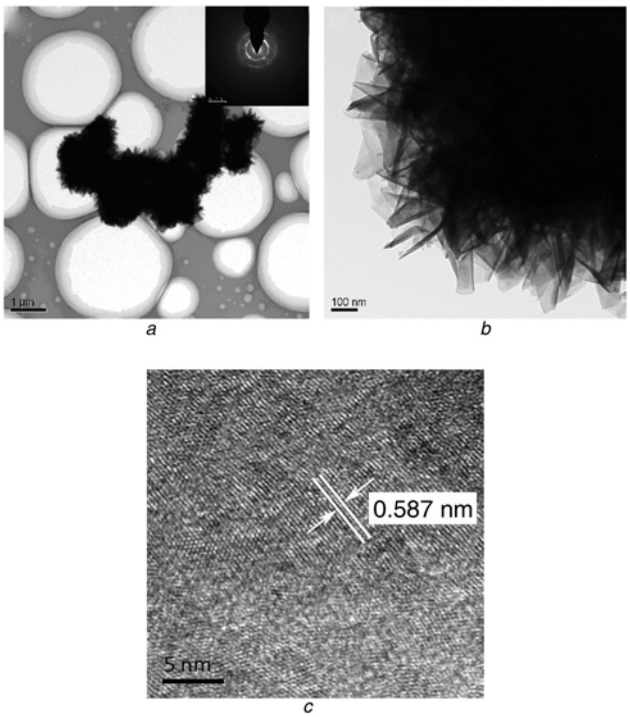

Figure 5 *TEM images (Fig. 5a, b) and SAED pattern (inset) of as-prepared $ZnIn_2S_4$ sample; HRTEM image taken at edge of single $ZnIn_2S_4$ microsphere (Fig. 5c); the 0.587 nm separation is for two spacings of (104) plane*

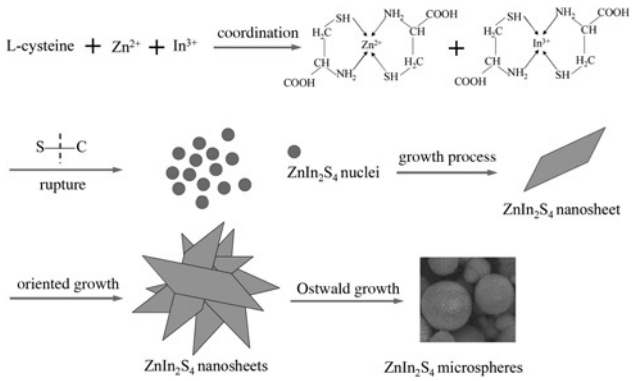

Figure 6 *Growth progress of nanosheet-built $ZnIn_2S_4$ microspheres in the presence of L-cysteine under hydrothermal conditions*

equations (1)–(3)

$$Zn^{2+} + n\text{L-cysteine} \xrightarrow{\text{coordination}} [Zn(\text{L-cysteine})_n]^{2+} \quad (1)$$

$$In^{3+} + n\text{L-cysteine} \xrightarrow{\text{coordination}} [In(\text{L-cysteine})_n]^{3+} \quad (2)$$

$$[Zn(\text{L-cysteine})_n]^{2+} + [In(\text{L-cysteine})_n]^{3+} \xrightarrow{\text{decomposition}} ZnIn_2S_4\text{nuclei} \quad (3)$$

$$ZnIn_2S_{4\,\text{nuclei}} \xrightarrow{\text{growth}} ZnIn_2S_{4\,\text{nanosheet-built microsphere}} \quad (4)$$

For the subsequent crystal growth step, the formed $ZnIn_2S_4$ nuclei firstly served as seeds to form small $ZnIn_2S_4$ nanosheets. Simultaneously, the boiling distilled water made these freshly formed nuclei mix homogeneously, which promoted the oriented growth of the $ZnIn_2S_4$ nanosheets [18–25, 28–33]. To minimise the total energy of the system, the small $ZnIn_2S_4$ nanosheets gathered together to form nanosheet-composed aggregates along the preferential growth axis under the hydrothermal conditions. With the prolongation of the reaction time, the nanosheet-built $ZnIn_2S_4$ microspheres finally formed through a typical Ostwald ripening process [18–25, 28–33]. This process could be described as the above equation (4) and be understood better with the help of the schematic diagram in Fig. 6. However, detailed and fundamental insight into the formation mechanism is still needed and some further investigations are under way because of the complexity of the L-cysteine-assisted hydrothermal ternary solution system.

4. Conclusions: A simple and mild green approach was developed for the preparation of nanosheet-built $ZnIn_2S_4$ microspheres by using L-cysteine as the sulphide source and complexing agent. The phase structure and composition of the product were tested by XRD, XPS and EDS. The morphologies and microstructure of the product were confirmed by FE-SEM, TEM and SAED, which show that the diameter of the microspheres and the thickness of the nanosheets are 100 nm–2 μm and 10–50 nm, respectively. This L-cysteine-assisted hydrothermal approach is simple, efficient and green and it would provide a general method for the preparation of other II–III–VI ternary metal sulphide crystals.

5. Acknowldgments: The authors acknowledge financial support from the National Natural Sciences Foundations of China (grant nos. 50972107 and 50772075).

6 References

[1] Li M.T., Su J.Z., Guo L.J.: 'Preparation and characterization of $ZnIn_2S_4$ thin films deposited by spray pyrolysis for hydrogen production', *Int. J. Hydrogen Energy*, 2008, **33**, pp. 2891–2896

[2] Lei Z.B., You W.S., Liu M.Y., *ET AL.*: 'Photocatalytic water reduction under visible light on a novel $ZnIn_2S_4$ catalyst synthesized by hydrothermal method', *Chem. Commun.*, 2003, **17**, pp. 2142–2143

[3] Gou X.L., Cheng F.Y., Shi Y.H., *ET AL.*: 'Shape-controlled synthesis of ternary chalcogenide $ZnIn_2S_4$ and $CuIn(S,Se)_2$ nano-/microstructures via facile solution route', *J. Am. Chem. Soc.*, 2006, **128**, pp. 7222–72229

[4] Hu X.L., Yu J.C., Gong J.M., Li Q.: 'Rapid mass production of hierarchically porous $ZnIn_2S_4$ sub-microspheres via a microwave-solvothermal process', *Cryst. Growth Des.*, 2007, **7**, (12), pp. 2444–2448

[5] Chen Z.X., Li D.Z., Zhang W.J., *ET AL.*: 'Photocatalytic degradation of dyes by $ZnIn_2S_4$ microspheres under visible light irradiation', *J. Phys. Chem. C*, 2009, **113**, pp. 4433–4440

[6] Shen S.H., Zhao L., Guo L.J.: 'Morphology, structure and photocatalytic performance of $ZnIn_2S_4$ synthesized via a solvothermal/hydrothermal route in different solvents', *J. Phys. Chem. Solids*, 2008, **69**, pp. 2426–2432

[7] Shen S.H., Zhao L., Guo L.J.: 'Crystallite, optical and photocatalytic properties of visible-light-driven $ZnIn_2S_4$ photocatalysts synthesized via a surfactant-assisted hydrothermal method', *Mater. Res. Bull.*, 2009, **44**, pp. 100–105

[8] Shen S.H., Zhao L., Guo L.J.: 'Cetyltrimethylammoniumbromide (CTAB)-assisted hydrothermal synthesis of $ZnIn_2S_4$ as an efficient visible-light-driven photocatalyst for hydrogen production', *Int. J. Hydrogen Energy*, 2008, **33**, pp. 4501–4510

[9] Li F., Luo J.H., Chen G.P., *ET AL.*: 'Hydrothermal synthesis of zinc indium sulfide microspheres with Ag^+ doping for enhanced H_2 production by photocatalytic water splitting under visible light', *Catal. Sci. Technol.*, 2014, **4**, pp. 1144–1150

[10] Shi L., Yin P.Q., Dai Y.M.: 'Synthesis and photocatalytic performance of $ZnIn_2S_4$ nanotubes and nanowires', *Langmuir*, 2013, **29**, pp. 12818–12822

[11] Chai B., Peng T.Y., Zeng P., Zhang X.H., Liu X.J.: 'Template-free hydrothermal synthesis of $ZnIn_2S_4$ floriated microsphere as an efficient photocatalyst for H_2 production under visible-light irradiation', *J. Phys. Chem. C*, 2011, **115**, pp. 6149–6155

[12] Wang A.J., Liao Q.C., Feng J.J., Zhang P.P., Zhang Z.M., Chen J.R.: 'D-Penicillamine-assisted self-assembly of hierarchical PbS microstars with octa-symmetric-dendritic arms', *Cryst. Growth Des.*, 2012, **12**, pp. 832–841

[13] Lu Q., Gao Y.F., Komarneni S.: 'Biomolecule-assisted synthesis of highly ordered snowflake like structures of bismuth sulfide nanorods', *J. Am. Chem. Soc.*, 2004, **126**, pp. 54–55

[14] Qiu W.M., Xu M.S., Yang X., *ET AL.*: 'Biomolecule-assisted hydrothermal synthesis of In_2S_3 porous films and enhanced photocatalytic properties', *J. Mater. Chem.*, 2011, **21**, pp. 13327–13333

[15] Yang X.F., Dong X.T., Wang J.X., Liu G.X.: 'Glycine-assisted hydrothermal synthesis of single-crystalline $LaF_3:Eu^{3+}$ hexagonal nanoplates', *J. Alloys Compd.*, 2009, **487**, pp. 298–303

[16] Hou L.R., Yuan C.Z., Yang L., Shen L.F., Zhang F., Zhang X.G.: 'Biomolecule-assisted hydrothermal approach towards synthesis of ultra-thin nanoporous α-$Co(OH)_2$ mesocrystal nanosheets for electrochemical capacitors', *Cryst. Eng. Commun.*, 2011, **13**, pp. 6130–6135

[17] Gao F., Lu Q.Y., Komarneni S.: 'Protein-assisted synthesis of single-crystal nanowires of bismuth compounds', *Chem. Commun.*, 2005, **2005**, (4), pp. 531–533

[18] Li B.X., Xie Y., Xue Y.: 'Controllable synthesis of CuS nanostructures from self-assembled precursors with biomolecule assistance', *J. Phys. Chem. C*, 2007, **111**, pp. 12181–12187

[19] Xiong S.L., Xi B.J., Xu D.C., *ET AL.*: 'L-cysteine-assisted tunable synthesis of PbS of various morphologies', *J. Phys. Chem. C*, 2007, **111**, pp. 16761–16767

[20] Min Y.L., Chen Y.C., Zhao Y.G.: 'A small biomolecule-assisted synthesis of iron sulfide nanostructures and magnetic properties', *Solid State Sci.*, 2009, **11**, pp. 451–455

[21] Chen L.Y., Zhang Z.D., Wang W.Z.: 'Self-assembled porous 3D flowerlike β-In_2S_3 structures: synthesis, characterization, and optical properties', *J. Phys. Chem. C*, 2008, **112**, pp. 4117–4123

[22] Chen X.Y., Li H.L., Wang S.M., Yang M., Qi Y.X.: 'Biomolecule-assisted hydrothermal synthesis of molybdenum disulfide microspheres with nanorods', *Mater. Lett.*, 2012, **66**, pp. 22–24

[23] Ma W., Chen G., Zhang D., Zhou K.C., Qiu G.Z., Liu X.H.: 'Biomolecule-assisted hydrothermal synthesis and properties of manganese sulfide hollow microspheres', *J. Phys. Chem. Solids*, 2012, **73**, pp. 1385–1389

[24] Chen G., Ma W., Zhang D., Zhu J.Y., Liu X.H.: 'Shape evolution and electrochemical properties of cobalt sulfide via a biomolecule-assisted solvothermal route', *Solid State Sci.*, 2013, **17**, pp. 102–106

doi: 10.1049/mnl.2014.0472

[25] Zhong J.S., Xiang W.D., Xie C.P., Liang X.J., Xu X.: 'Synthesis of spheroidal $AgBiS_2$ microcrystals by L-cysteine assisted method', *Mater. Chem. Phys.*, 2013, **138**, pp. 773–779
[26] Chang K., Chen W.X.: 'L-cysteine-assisted synthesis of layered MoS_2/graphene composites with excellent electrochemical performances for lithium ion batteries', *ACS Nano*, 2011, **5**, (6), pp. 4720–4728
[27] Chen Z.X., Li D.Z., Zhang W.J., *ET AL.*: 'Low-temperature and template-free synthesis of $ZnIn_2S_4$ microspheres', *Inorg. Chem.*, 2008, **47**, pp. 9766–9772
[28] Burford N., Eelman M.D., Mahony D.E., Morash M.: 'Definitive identification of cysteine and glutathione complexes of bismuth by mass spectrometry: assessing the biochemical fate of bismuth pharmaceutical agents', *Chem. Commun.*, 2003, **7**, pp. 146–147
[29] Shen G.Z., Chen D., Tang K.B., Qian Y.T.: 'Synthesis of ternary sulfides Cu(Ag)–Bi–S coral-shaped crystals from single-source precursors', *J. Cryst. Growth*, 2003, **257**, pp. 293–296
[30] Shen G.Z., Chen D., Tang K.B., Qian Y.T.: 'Novel polyol route to $AgBiS_2$ nanorods', *J. Cryst. Growth*, 2003, **252**, pp. 199–201
[31] Chen D., Shen G.Z., Tang K.B., Liu X.M., Qian Y.T., Zhou G.E.: 'The synthesis of Cu_3BiS_3 nanorods via a simple ethanol-thermal route', *J. Cryst. Growth*, 2003, **253**, pp. 512–516
[32] Chen D., Shen G.Z., Tang K.B., *ET AL.*: 'Microwave synthesis of $AgBiS_2$ dendrites in aqueous solution', *Inorg. Chem. Commun.*, 2003, **6**, pp. 710–712
[33] Thongtema T., Tipcompor N., Thongtem S.: 'Characterization of $AgBiS_2$ nanostructured flowers produced by solvothermal reaction', *Mater. Lett.*, 2010, **64**, pp. 755–758